Nanoscale

Accepted Manuscript

Check for updates

Volume 8 | Number 1 | 7 January 2016 | Pages 1–660

Nanoscale

www.rsc.org/nanoscale

ISSN 2040-3364

ROYAL SOCIETY OF CHEMISTRY

PAPER
Qian Wang et al.
TiC₂ a new two-dimensional sheet beyond MXenes

NCNST

ROYAL SOCIETY OF CHEMISTRY

rsc.li/nanoscale

ROYAL SOCIETY
OF CHEMISTRY

Journal Name

ARTICLE

A Novel Fluorescent Adhesive-assisted Biomimetic Mineralization

Zhe Wang, [a,b] Yan Ouyang, [a] Zhifang Wu, [a,b] Leiqing Zhang, [a,b] Changyu Shao, [c] Jiayan Fan, [a,b] Ling Zhang, [a,b] Ying Shi, [a,b] Zihuai Zhou, [a,b] Haihua Pan, [d] Ruikang Tang, [c,d] and Baiping Fu,*[a,b]

We propose a novel fluorescent adhesive-assisted biomimetic mineralization strategy, based on which 1 wt % of sodium fluorescein and 25 wt % of polyacrylic acid stabilized amorphous calcium phosphate (PAA-ACP) nanoparticles were incorporated into a mild self-etch adhesive (Clearfil S3 Bond) as a fluorescent mineralizing adhesive. The characterizations of the PAA-ACP nanoparticles indicate that they were spheric particles clustered together, each particle in a diameter of approximately 20~50 nm, in a metastable phase with two characteristic absorption peaks (1050 cm^{-1} and 580 cm^{-1}). Our results suggest that the fluorescent mineralizing adhesive was non-cytotoxic with minimal esthetic interference and its fluorescence intensity did not significantly decrease within 6 months. Our data reveal that the fluorescent mineralizing adhesive could induce the extra- and intra-fibrillar remineralization of the reconstituted type I collagen, the demineralized enamel and dentin substrate. Our data demonstrate that a novel fluorescent adhesive-assisted biomimetic mineralization strategy will pave the way to design and produce anti-carious materials for the prevention of dental caries.

1. Introduction

Dental caries is one of the most prevalent human diseases worldwide.[1] Dental caries starts to occur once demineralization of tooth hard tissues is faster than remineralization in a state of biofilm dysbiosis caused by cariogenic bacteria.[2] If dental caries is not treated in time, it will continue to decay the tooth hard tissues, and result in pulpitis, osteomyelitis and even worse complications.[3]

Minimally invasive dentistry (MID) advocates to prevent and even reverse initial caries (non-cavitated lesions) by means of contemporary nanotechnology and nanomaterials.[4] In near future, non-cavitated lesions are expected to be completely reversed by biomimetic mineralization strategies.[5] During the biomimetic mineralization process, amorphous calcium phosphate (ACP) is believed to be a liquid-precursor of hydroxyapatite.[6] Unlike the traditional classical pathway of ion-mediated crystallization,[7] non-collagenous protein analogues (NCPs) such as polyacrylic acid (PAA), poly(amidoamine) (PAMAM), and L-glutamic acid (L-Glu) have been proven to play an important role in inducing ACP nanoparticles to remineralize type I collagen, demineralized enamel and dentin in mineralization solutions or simulated body fluid (SBF).[8-11] In this process, ACP nanoparticles undergo as pre-nucleation clusters.[12, 13] The pre-nucleation clusters aggregate each other into larger ones, which penetrate into collagen fibrils and self-assemble to form crystalline phase by mediation of NCPs.[14, 15] That is so called non-classical crystal theory.[16] Based on the theory, numerous reports revealed that solution-based carrier to deliver the biomimetic mineralization successfully resulted in the heavy mineralization of collagen fiber, demineralized enamel and dentin in laboratory.[17-19] Likewise, paste- or gel-based carrier for ACP nanoprecursors has also been reported to induce the remineralization in vitro and vivo study.[11, 20-22] Contemporary commercial anti-carious materials are available in the form of liquids and pastes such as mouthrinse and toothpaste. Their remineralization effects are mainly based on polymer-induced liquid-precursor (PILP).[23, 24] However, their clinical remineralization effectiveness is not so good as expected to efficiently reverse the non-cavitated carious lesions.[18] That might be attributed to the lack of continuously-provided calcium and phosphate resources for caries prevention.[25] The prevention and reversal of non-cavitated carious lesions might be achieved by biomimetic mineralization strategies, which need periodic or continuous replenishment with the sufficient calcium and phosphate resources.[26]

Our pilot study revealed that the self-etch adhesive could be used as a carrier loaded with Si-ACP nanoprecursors to deliver biomimetic mineralization.[27] A question is raised whether the self-etch adhesive can be used as a universal carrier loaded with other nanoprecursors such as PAA-stabilized ACP (PAA-ACP) nanoparticles to inspire the remineralization. Furthermore, the applications of mineralizing materials on tooth surfaces are expected to be detectable with the minimal esthetic interference of tooth color. The retention

a. Department of Prosthodontics, Hospital of Stomatology Affiliated to Zhejiang University School of Medicine, Hangzhou 310006, Zhejiang, China;

b. Key Laboratory for Oral Biomedical Research of Zhejiang Province, Hangzhou, 310020, Zhejiang, China

c. Center for Biomaterials and Biopathways, Department of Chemistry, Zhejiang University, Hangzhou 310027, Zhejiang, China.

d. Qiushi Academy for Advanced Studies, Zhejiang University, Hangzhou 310027, Zhejiang, China.

ARTICLE

of mineralizing materials should be associated with the effective prevention of dental caries.[28] The sodium fluorescein is non-toxic and widely used as contrast agent in ophthalmology.[29] It has been applied to indicate tumor boundary during general surgical operation.[30] To date, nobody knows whether the mineralizing materials and fluorescent agent will be influenced by each other if sodium fluorescein and ACP nanoparticles are incorporated into a self-etch adhesive. Therefore, we propose a novel fluorescent adhesive-assisted biomimetic mineralization strategy based on a novel fluorescent mineralizing adhesive. The remineralization effects and the changes of fluorescence intensity should be investigated in detail. It is eager to determine which kinds of phrase transformation of the remineralization occur on the demineralized enamel and dentin, solid-solid transformation or dissolution-precipitation, when the novel fluorescent adhesive-assisted biomimetic mineralization strategy used. The aim of this study was to investigate 1) the feasibility of a novel fluorescent adhesive-assisted biomimetic mineralization strategy, namely, its remineralizaiton effects, fluorescence intensity and cell toxicity; and 2) the phrase transformation process of ACP nanoparticles on the demineralized dentin and enamel.
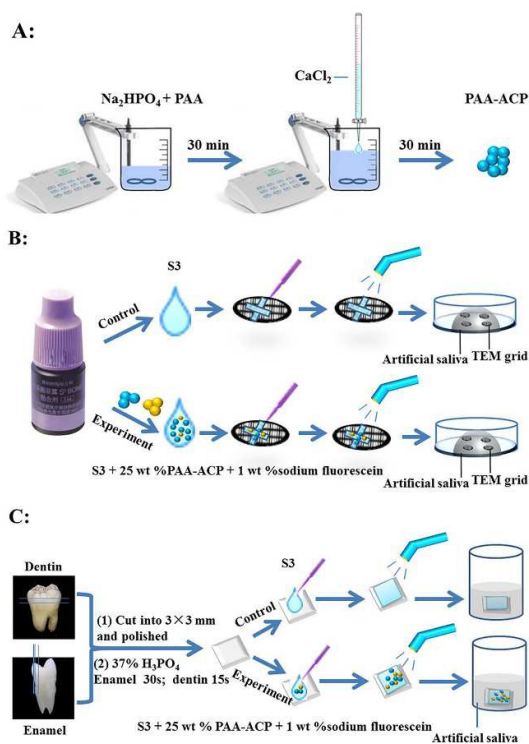

Fig. 1 Simplified diagram of the methodology of specimen preparation. A: Synthesis of PAA-ACP nanoparticles. B: A cross was brushed on a collagen-coated grid either with the experimental adhesive (S3+25 wt % PAA-ACP + 1 wt % sodium fluorescein) or with the adhesive S3 for mineralization test. C: Mineralization of demineralized enamel and dentin that were treated either with the experimental adhesive or with the adhesive S3.

2. Experiments

All the chemicals used in this study were commercially purchased , and were of analytical chemical grade. They included $CaCl_2$, Na_2HPO_4, polyacrylic acid (PAA, average Mw=1800), NaN_3, glycine, sodium fluorescein, and 4-(2-hydroxyethyl)- 1-piperazineethanesulfonic acid (HEPES) from Sigma-Aldrich, USA; KCl, 50 wt% of glutaraldehyde, NaOH, 37wt% of H_3PO_4, uranyl acetate and KH_2PO_4 from Aladdin, China. All the solutions were filtered through 0.22 μm Millipore membranes (USA) before use. Rat tail type I collagen solution was obtained from Gibco, Invitrogen, USA. The simplified diagram of the methodology of specimen preparation is shown in Fig. 1.

2.1 Synthesis and characterization of PAA-ACP nanoparticles

The PAA-ACP nanoparticles were synthesized as follows: Twenty-five mL phosphate solution containing 12 mM Na_2HPO_4 and 700 μg/mL PAA (MW: 1800) was magnetically being stirred at room temperature for 30 min and the pH of the solution was titrated to 9.5 ± 0.1 with 1 M NaOH. Subsequently, the equal volume of calcium solution containing 20 mM $CaCl_2$ was successively being dripped into the phosphate solution via a burette in 30 min, and the pH of the mixed solution was re-titrated to 9.5 ± 0.5 with 0.1 M NaOH. Afterward, precipitates of PAA-ACP nanoparticles were collected by centrifugation (16000 rpm, 5 min, Beckman Allegra64R, USA), and washed three times with absolute ethanol. Then, the PAA-ACP nanoparticles were dried under vacuum at 30 °C overnight. Finally, the PAA-ACP nanoparticles were analyzed by scanning electron microscopy (SEM, HITACHI, SU8010, Tokyo, Japan), Fourier transform infrared spectroscopy (FTIR, Spectrum 400, Perkin-Elmer, USA), transmission electron microscopy (TEM, JEM-1230, JEOL, Tokyo, Japan) and X-ray diffraction (XRD, Rigaku D/MAX-2550pc, Japan).

2.2 Preparation of the experimental adhesive

One-bottle mild self-etch adhesive Clearfil S3 Bond (S3, Kuraray-Noritake, Japan) was used as control. A fluorescent mineralizing adhesive as an experimental adhesive was prepared by the incorporation of 25 wt % of PAA-ACP nanoparticles and 1 wt % of sodium fluorescein into the adhesive S3.

2.3. Fluorescence test

2.3.1 Fluorescence qualitative test

Two occlusal surfaces of human third molars were applied either with the adhesive S3 or with the experimental adhesive, agitated for 20 s, air-dried for 10 s, and light-cured with a LED-blue light-curing unit (Woodpacker, 1500 mW/cm^2, China) for 40 s, each quadrant for 10 s, respectively. Then the photos of

two occlusal surfaces were taken 30 cm away from the occlusal surfaces with a camera (Nikon, Viltrox JY-670 Macro Ring Lite, Japan) through the eye shield when they were irradiated by the light-curing unit. The fluorescence was blindly determined by a dentist to read the photos via naked eyes.

2.3.2 Fluorescence intensity qualitative test

The experimental adhesive and the adhesive S3 were each dropped into a metal ring with an inner diameter of 1 cm and height of 0.1 mm, light-cured for 40 s, each quadrant for 10 s, respectively, in order to produce the adhesive films. Forty-eight films, 24 each adhesive, were prepared. Fluorescence intensity tests of the all films, six each subgroup, were performed with fluorescence spectrophotometer (RF-5301PC, Shimadzu, Japan), immediately, 1, 3 and 6 months after they were stored in 12 mL of monthly-changed artificial saliva (1.5 mM $CaCl_2$, 0.9 mM KH_2PO_4, 130 mM KCl, 1.0 mM NaN_3, and 20 mM HEPES, pH 7.0) at 37°C.

2.4 Mineralization capability of the experimental adhesive

The mineralization capability of the experimental adhesive was determined using reconstituted type I collagen fibrils, demineralized enamel and dentin disks. The preparation of the reconstituted type I collagen fibrils, the demineralized enamel/dentin disks and their remineralization samples for TEM, confocal laser- scanning microscopy (CLSM) and X-Ray Diffraction (XRD) were described in the ESI†.

2.4.1 Mineralization of reconstituted type I collagen fibrils

A total of 24 collagen-coated grids were prepared and randomly divided into two groups. A cross was gently brushed on a collagen-coated grid either with the adhesive S3 or with the experimental adhesive, gently air-dried and light-cured, respectively (Fig. 1B). Four grids each group floating upside-down on 60 μL of artificial saliva were incubated in a 100% of humidity chamber at 37 °C for 1, 4, and 7 days before they were retrieved, and rinsed with deionized distilled water, 50% of ethanol and absolute ethanol in turn. Then they were dried in the air, and analyzed by TEM (JEM-1230, JEOL, Tokyo, Japan) with selected area electron diffraction (SAED) and high resolution transmission electron microscopy (HRTEM, JEM-2100F, JEOL, Tokyo, Japan) with Mapping.

2.4.2 Mineralization of demineralized enamel and dentin

The demineralized enamel/dentin disks (n=20) were applied either with the adhesive S3 or with the experimental adhesive, agitated for 20 s, gently air-dried for 10 s, and light-cured for 40 s, respectively. Subsequently, all samples, four each subgroup, were incubated in 4 mL of weekly-changed artificial saliva in a 100% of humidity chamber at 37 °C for 2 and 4 wks before they were retrieved and prepared for ultrathin sections. Finally, they were analyzed with TEM, SAED, HRTEM and Mapping. The surfaces of another four enamel/dentin samples were further analyzed by CLSM and XRD, immediately and 4 wks of storage in artificial saliva after the demineralized

enamel and dentin surfaces were applied with the experimental adhesive.

2.5. Cytotoxicity test

The cytotoxicity of the experimental adhesive was assessed by Cell Counting Kit-8 (CCK-8) assay (Beyotime, Shanghai, China). The above-mentioned adhesive films prepared at different concentrations of 1, 2, 4 mg/mL were incubated in Duibecco's modified Eagle's medium (DMEM, Gibco, USA), which was supplemented with 10% of fetal bovine serum (FBS, Gibco, USA) at 37 °C for 24 hrs to obtain leach solutions. Then, the L929 cells (Shanghai Cell Collection, China) were seeded in 96 well plates with a density of 1.0×10^4/well and allowed 24 hrs to adhere to the surface of each well. Subsequently, the attached cells were incubated at 37°C in humidified 5% CO2 atmosphere with the different leach solutions for 24 hrs . Afterwards, 10 μL CCK-8 was added into each well and incubated for another 2-3 hrs. The absorbance at 450 nm was measured with a microplate reader (Bio Tek Eon) for six times.

Results and Discussions

3.1 Characterization of PAA-ACP nanoparticles

ACP nanoparticles are believed to be unstable in solution due to easy transformation to HAp.[31] They could be stabilized by
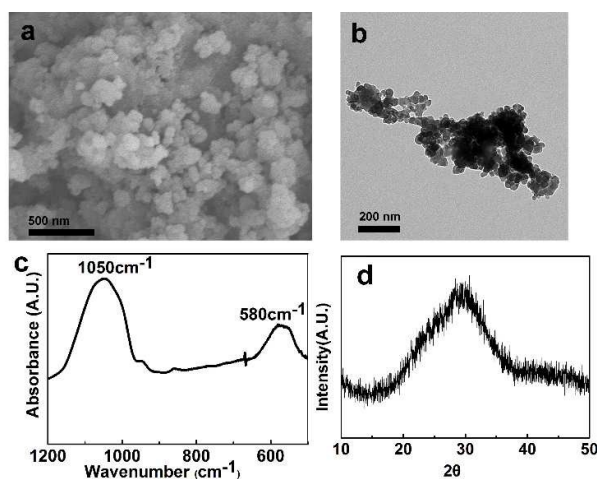

Fig. 2 Characterization of PAA- ACP nanoparticles. a: SEM image shows that the round PAA-ACP nanoparticles cluster together. b: TEM image shows that the PAA-ACP nanoparticles are in a diameter of approximately 20-50 nm. c: FTIR Spectrum of PAA-ACP nanoparticles shows two characteristic absorption peaks PO_4^{3-} at 1050 cm^{-1} and 580 cm^{-1}. d: XRD indicates an amorphous state of PAA-ACP nanoparticles at 2θ= 30°.

NCPs, inorganic ions and surface modification in a metastable phase.[8, 32, 33] The SEM and TEM images show that PAA-ACP nanoparticles are spherical particles with a diameter of approximately 20-50 nm (Fig. 2 a, b). According to a previous study, ACP nanoparticles smaller than 40 nm could easily infiltrate into the gap zone of collagen fibrils, in which they

ARTICLE

could initiate nucleation formation of HAp.[34] Thus, it is inferred that most of PAA-ACP nanoparticles (20-50 nm) in this study could penetrate into the gap zone of collagen fibrils to form the intrafibrillar mineralization.[35] The FTIR spectrum of PAA-ACP nanoparticles reveals two characteristic absorption peaks of PO_4^{3-} at 1050 cm^{-1} and 580 cm^{-1} (Fig. 2 c). A single peak at 580 cm^{-1} is the characteristic of the amorphous phase (Fig. 2 c). Once ACP has been transformed to HAp, the peak at 580 cm^{-1} will be split into two peaks at 600 cm^{-1} and 560 cm^{-1}.[10] The XRD spectrum of PAA-ACP nanoparticles shows a broad peak of 2θ=30°, also indicating the amorphous phase (Fig. 2 d).[36] Taken together, PAA-ACP nanoparticles in this study were believed to be in a metastable phase at the initial stage of mineralization.[3,10]

3.2 The qualitative and quantitative fluorescence tests of the experimental adhesive

Photographs of two occlusal surfaces reveal that the occlusal surface treated with the experimental adhesive looks yellowish under natural light along occlusal fissures, and obviously fluorescent along occlusal fissures through an eye shield under the LED-blue light (Fig. 3 a, b), while the occlusal surface treated with the adhesive S3 looks a little bit yellowish but no visibly fluorescent (Fig. 3 b, d). The retention of dental restorative materials is directly associated with the effectiveness in caries prevention.[28, 38] It is very easy for dentists to detect the retention of the fluorescent tooth-colored restorative materials.
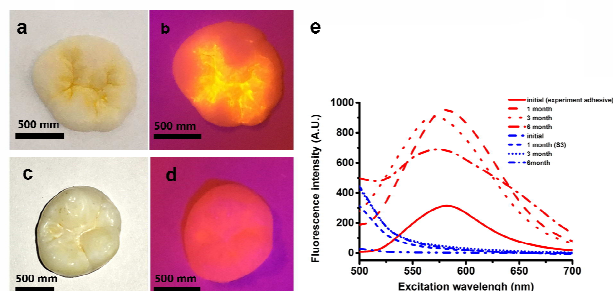

Fig. 3 Two occlusal surfaces treated with the experimental adhesive (panels a and b) or the adhesive S3 (panels c and d). The fluorescence intensity (Means) of the experimental adhesive and adhesive S3 films were measured, immediately, and 1, 3 and 6 months after storage in artificial saliva (panel e). Red line: the experimental adhesive. blue line: adhesive S3.

The fluorescence intensity of the experimental adhesive did not dramatically decrease within 6 months (Fig. 3, e, red lines). The fluorescence of adhesive S3 was not detected (Fig. 3, e, blue lines). Sodium fluorescein has six different tautomers, and each tautomer is in a condition of acid-base equilibrium.[39] When the concentration of dianion in all tautomers gradually increases with the increase of pH values in the solution, the laser energy conversion efficiency of sodium fluorescein solution will be increased with the increasing dianion.[39, 40] The fluorescence intensity of the light-cured, acidic experimental adhesive increased at the first 3 months,

and slightly decreased at the end of sixth month (Fig. 3 e). It is completely consistent with the inference based on increasing concentrations of dianions of sodium fluorescein,[39, 41] in which the pH value of the self-etch adhesive was increased with the polymerization of the adhesive.

3.3 Mineralization of reconstituted type I collagen fibrils

The reconstituted type I collagen covered on the grids has been used as an ideal model for rapid screening of mineralization potentials (Fig. S1).[8, 34] The TEM images reveal that type I collagen fibrils became significantly thicker after the grids treated with the experimental adhesive were incubated in artificial saliva for 1 day (Fig. 4 a, b). PAA-ACP nanoparticles were seen adhering to the external side of the type I collagen fibrils (Fig. 4 a, b). The banding structure of type I collagen fibrils was visible (Fig. 4 b). The SAED pattern reveals an amorphous state (Fig. 4 b). After 4 days of incubation, most of the intra- and extra-fibrils were mineralized (Fig. 4 c, d). PAA-ACP nanoparticles might infiltrate into collagen gap zone and
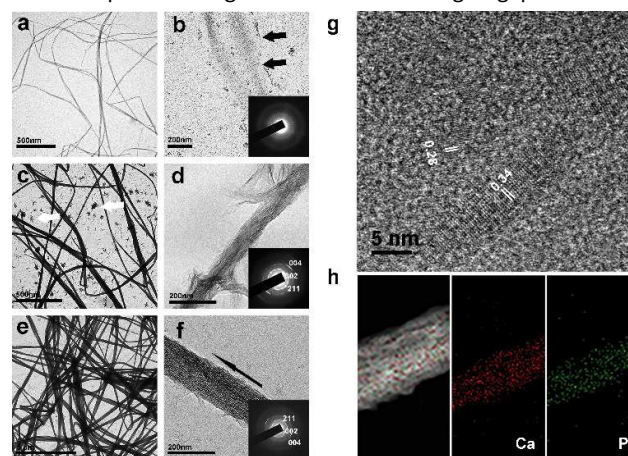

Fig. 4 TEM images of the mineralization of the reconstituted type I collagen fibrils. A cross was painted on a collagen-covered grid with the experimental adhesive and light-cured. The grids were incubated in artificial saliva for 1 (panels a, b), 4 (panels c, d) and 7 (panels e, f) days. The collagen fibrils were attached by a small amount of ACP nanoparticles (panels b, black arrow). The SAED patterns (insets in panels b) indicate that the mineral phase was non-crystalline. Most of the collagen fibrils were mineralized after 4-day incubation (panels c, d), and extrafibrillar mineralization also occurred (white arrow). Almost all of the collagen fibrils were mineralized after 7-day incubations (panels e, f) Black arrow shows the crystallites are aligned along the longitudinal axis of the collagen fibrils (panel f). The SAED patterns (insets in panels d, f) indicate that the intrafibrillar mineral phase is apatite. HRTEM images of the 7-day samples indicate two interplanar spacing: 0.34 nm and 0.28 nm (panel g). The mapping of collagen fibrils of the 7-day samples indicate the homogenous distribution of calcium and phosphate elements (panel h)

transform to HAp. The type I collagen fibrils were heavily mineralized after incubation for 7 days (Fig.4 e, f). The HAp grew along the longitudinal axis of the collagen fibrils (black arrow) and filled the whole intrafibrillar spaces (Fig. 4 f). The banding structure of collagen became undistinguished due to the heavy mineralization (Fig. 4 e, f). The SAED patterns show that the c-axis of the intrafibrillar minerals was oriented along

the collagen axis within the 002, 004 and 211 planes (Fig. 4, insets in panels d, f). The results of TEM and SAED in this study are complete in agreement with the previous report.[42] HRTEM of the remineralized collagen shows inter-planar spacing of approximately 0.34 nm and 0.28 nm (Fig. 4 g).[43] This is completely consistent with the lattice fringes of 002 and 211 planes (Fig. 4 f), respectively. The mapping of the 7 days of mineralization collagen area also indicates that calcium and phosphorus elements were overlapped with each other, and uniformly distributed throughout the whole collagen fibrils (Fig. 4 h).

The findings in this study are fully consistent with the previous reports concerning intrafibrillar mineralization of collagens.[42-44] In addition, mineralization was not detected in the control group (S3), which might be resulted from the lack of nanoprecursors such as PAA-ACP nanoparticles (Fig. S2).[45] We confirmed our previous report concerning self-etch adhesive as a carrier for ACP nanoprecursors to deliver the biomimetic mineralization.[27] Furthermore, PAA-ACP nanoparticles could also play a positive role in the remineralization process. The ACP particles have been believed to serve as a reservoir of calcium and phosphate.[46] It is reasonably assumed that other ACP nanoparticles such as the PAA-ACP nanoparticles could also induce the extra- and intra-fibrillar mineralization along with the self-etch adhesive used as a universal carrier. Moreover, sodium fluorescein in the experimental adhesive not only did not interfere with the potential mineralization of collagen fibrils induced by PAA-ACP precursors (Fig. 4 c-f), but also could be easily detected in clinical condition (Fig. 3).

3.4 Mineralization of the Teeth

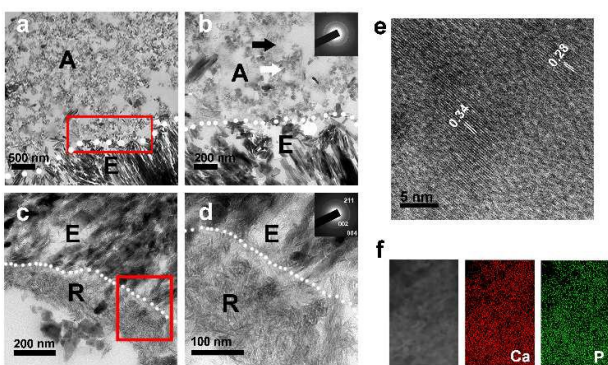For enamel mineralization, Fig. 5 a, b reveals that amount of

Fig. 5 TEM images of enamel treated with the experimental adhesive after 2 wks (panels a, b) and 4 wks (panels c, d) of storage in artificial saliva. White arrow indicates that ACP nanoparticles aggregate each other. Black arrow indicates that some ACP nanoparticles have became larger, some of which have transformed into HAp. SAED pattern shows the discrete ring patterns with the characteristic of hydroxyapatite (insets in panel b). A mineralized layer in situ is visible on the surface of the demineralized enamel (panels c, d). The SAED patterns reveal the 002, 004 and 211 rings (insets in panel d). HRTEM of 4-wk samples indicates two inter planar spacing: 0.34 nm and 0.28 nm (panel e). The mapping of 4-wk samples shows uniform distribution of Ca and P elements (panel f). E: enamel; A: adhesive; R: remineralization layer.

ACP nanoparticles are visible within the experimental adhesive layer, some of which have been transformed to HAp after 2-wk incubation (Black arrow in panel b). SAED pattern (insert in Fig. 5 b) reveals that the discrete ring patterns are characteristic of hydroxyapatite. A remineralization layer of approximately 200 nm in the vicinity of the enamel was detectable after 4-wk incubation (Fig. 5 c, d). The remineralization layer might be attributable to the transformation of ACP nanoparticles.[47] The SAED pattern (inserts in Fig. 5 d) shows the rings of the 002, 004 and 211, indicating crystalline phase. For dentin mineralization, the TEM images show that a remineralization layer was increased from approximately 100~200 nm to 400~500 nm on the base of intact dentin after the demineralized dentin treated with the experimental adhesive was incubated for 2 and 4 wks (Fig. 6 a-c, d-f). The SAED patterns (inserts in Fig. 6 c, f) show the discrete rings of 002, 211, and 004, indicating crystallite phase. The enamel and dentin samples incubated for 4 wks were further analyzed by HRTEM. The HRTEM images indicate two interplanar spacing: 0.34 nm and 0.28 nm, which are consistent with HAp lattice plane of 002 and 211 (Fig. 5 e. 6 g).[43] The Mapping also shows the uniform distribution of calcium and phosphorus elements (Fig. 5 f, 6 h). However, the remineralization layer was not found in the control group (adhesive S3) after the demineralized enamel/dentin samples were incubated for 2 and 4 wks (Fig. S3, S4). Thus, the limited calcium and phosphate ions in the artificial saliva could not induce mineralization in the control group since the amount of ACP is directly associated with the nucleation of HAp.[48]
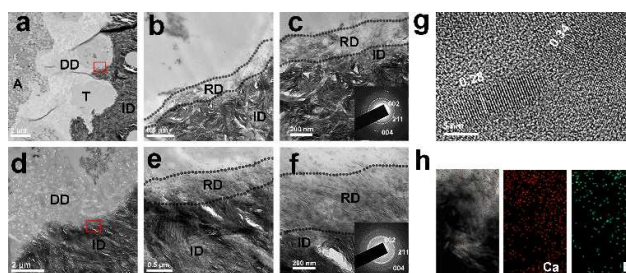

Fig. 6 The TEM images of demineralized dentin treated with the experimental adhesive after 2 wks (Panels a-c) and 4 wks (Panels d-f) of storage in artificial saliva. Panels b, e and c, f are the magnified views of panels a, d within red squares, respectively. The remineralization layer was increased from approximately 100-200 nm (2 wks) to 400-500 nm (4 wks). The SAED patterns (insert in panels c, f) reveal the characteristics of crystallites with the diffraction rings 002, 004, 211. A: adhesive. T: dentin tube. DD: demineralized dentin. ID: intact dentin. RD: remineralization dentin. HRTEM of 4-wk samples shows two interplanar spacing: 0.34 nm and 0.28 nm (panel g). The mapping of 4-wk samples reveals the uniform distribution of calcium and phosphorus (panels h).

PAA-ACP nanoparticles attached to the enamel surface by means of the experimental adhesive could form an immediate protective layer and gradually initiate nucleation in situ to be converted to HAp via solid-solid transformation.[49] The hydrophilic monomers of the adhesive such as hydroxyethyl methacrylate (HEMA) could adsorb water to produce hydrophilic zone at the interfaces of adhesive-enamel/dentin.[50, 51] The ACP nanoparticles might be stabilized

ARTICLE

by PAA at the initial stage, and gradually transformed to HAp in situ in the hydrophilic zone. This process was similar to a previous report that a solid-solid in situ transformation layer was detected on enamel surface.[52] This enamel remineralization process might undergo as follows: PAA-ACP nanoparticles aggregated each other at initial stage (Fig. 5 b white arrow). Subsequently, they became larger, some of which gradually transformed into nanocrystals (Fig. 5 b black arrow). The primary nanocrystals were closely stuck to each other and self-assembled into needle-like HAp by mediation of the PAA (Fig. 5 d). Finally, they formed a mineralized layer composed of needle-like HAp on the surface of the demineralized enamel (Fig. 5 c, d). This process is the same as the solid-solid phase transformation of amorphous calcium carbonate (ACC).[53-55]

On the contrary, the demineralized dentin might be remineralized in dissolution-reprecipitate process.[56] Since solid ACP nanoparticles (40 nm) were not detected midway between the experiment adhesive layer and the remineralization layer (Fig. 6 a-f). This remineralization process of the demineralized dentin in this study might undergo as follows: ACP nanoparticles were dissolved into calcium and phosphate ions. Subsequently, the ions could be attracted by counterpart ions (nucleation sites) to migrate through the demineralized collagen layer to the bottom of the demineralized dentin. Finally, they self-assembled to form nanocrystallites under the mediation of the PAA. Afterward, nanocrystallites gradually transformed into crystallites to form complete intra-fibrillar mineralization of dentin collagens.[45, 56] According to previous study, for enamel, the crystallite seeds are homogeneous HAp.[57] The crystallites directly nucleated and grew on the surface of the enamel HAp crystallites in inorganic environment.[58] However, the remineralization of the demineralized dentin were based on the collagen matrix, which is an organic-mediated process with heterogeneous crystallite seeds.[59] These findings in this study further confirmed the different remineralization processes of enamel and dentin when the fluorescent mineralizing self-etch adhesive used. However, the detail molecular mechanism of crystallization process of ACP nanoparticles into HAp needs to be further studied. Furthermore, the remineralization layers of enamel and dentin in this study were not exactly the same as micro-structure and density of natural enamel and dentin (Fig. 5, 6). It might be resulted from the limited amounts of ACP nanoparticles in one layer of adhesive.[48]

The CLSM images of the enamel/dentin samples show the fluorescent adhesive penetrates into approximately 20-30 μm of the demineralized enamel and approximately 50-60 μm of the demineralized dentin. Thus, ACP nanoparticles can penetrate into the demineralized enamel/dentin along with the adhesive at the initial stage of the remineralization, which is beneficial to induce teeth mineralization (Fig. S5). However, the boundaries between the original teeth and the remineralized layer could not be detected by the CLSM due to the nanoscale remineralization in this study (Fig. S5 b, d). Contrarily, the XRD spectra of re- and de-mineralized enamel and dentin indicate the same peaks such as 002, 211, 112 and

300 (Fig. 7 a, b), demonstrating to be HAp.[60] Furthermore, XRD spectrum shows a broad peak at 2θ = 20-30° immediately after the demineralized enamel and dentin surfaces were applied with fluorescent mineralizing adhesive, indicating that PAA-ACP nanoparticles within the experimental adhesive were amorphous phase at beginning of remineraliztion.[61] Thus, the XRD spectra further confirm the remineralization on the surfaces of the de-mineralized enamel/dentin.
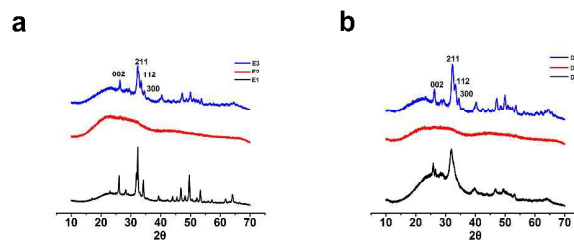

Fig. 7 XRD spectra of the de- and re-mineralized enamel/dentin disks. The de-mineralized enamel/dentin disks were etched with 37% of phosphoric acid, enamel (E1) for 30 s and dentin (D1) for 10 s. The enamel/dentin samples were determined by XRD, immediately after etching (E1, D2), immediately (E2, D2) and 4 wks of storage in artificial saliva (E3, D3) after they were applied with the experimental adhesive. a: enamel. b: dentin

Taken together, the TEM, HRTEM, SAED, Mapping images and XRD patterns confirmed that the nanocrystallites in the remineralization layer were HAp. The degree of collagen mineralization could be increased with the increasing amount of ACP nanoparticles in the self-etch adhesive (Fig. S 6). That imply that the novel fluorescent adhesive-assisted biomimetic remineralization strategy might be promising for prevention and reversal of non-cavitation lesions.

3.5 The cytotoxicity of the experimental adhesive

As cytotoxicity test is a key step in assessing the biocompatibility of materials in biomedical applications. The results of CCK-8 assay show that the experimental adhesive is
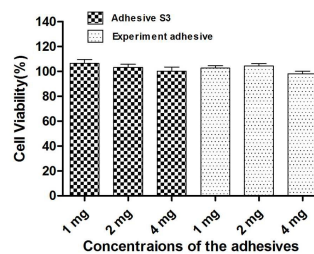

Fig. 8 Cytotoxicity of the films of the experimental adhesive and the adhesive S3 at different concentrations.

non-cytotoxic and good biocompatible (Fig. 8). This study is completely consistent with previous studies,[62,63] demonstrating that the adhesive materials containing ACP nanoparticles possess the favorable biocompatibility.

3. Conclusions

Journal Name

ARTICLE

According to the limited data in this study, the conclusions could be drawn as follows: The novel fluorescent adhesive-assisted biomimetic mineralization strategy, based on the fluorescent mineralizing adhesive composed of 25 wt % of PAA-ACP nanoparticles, 1 wt % of sodium fluorescein and the mild self-etch adhesive (Clearfil S3 Bond), could induce the extra- and intra-fibrillar remineralization of the reconstituted type I collagen, the demineralized enamel and dentin as well as possess the excellent biocompatibility and the detectable fluorescence of the minimal esthetic interference of tooth color. This strategy will pave the way to design and produce anti-carious materials for the prevention of dental caries.

Live Subject Statement

All experiments were performed in accordance with the International Ethical Guidelines of the Declaration of Helsinki (World Medical Association, 2008)1 and National Ethics Censorship of Biomedical Research Involving Human Subject.2 The freshly-extracted human teeth (premolars extracted for orthodontic reason and third molars) were collected with the patient's informed consent. The protocol was approved by the Ethical Committee of Hospital of Stomatology Affiliated to Zhejiang University School of Medicine (No. 201708).

1. Introduction A. WMA Declaration of Helsinki - Ethical Principles for Medical Research Involving Human Subjects. World Medical Journal, 2008, 27(2):235-237.

2. No. 11 Bulletin of National Health Commission of People's Republic's of China, 2016,http://www.moh.gov.cn/fzs/s3576/201610/84b33b81d8 e747eaaf048f68b174f829.shtml

Conflicts of interest

The all authors have declared no conflicts of interest..

Acknowledgements

References

1 R. H. Selwitz, A. I. Ismail and N. B. Pitts, *Lancet*, 2007, 369, 51-59.

2 L. Cheng, J. Li, H. H. K. Xu and X. Zhou, *Demineralization and Remineralization*, Springer Berlin Heidelberg, 2016.

3 A. Kishen, *Nanotechnology in Endodontics*, Springer International Publishing, 2015.

4 D. Elkassas and A. Arafa, *Nanomedicine: nanotechnology, biology, and medicine*, 2017, 13, 1543-1562.

5 J. D. Featherstone, M. Fontana and M. Wolff, *J. Dent. Res*, 2018, 97, 125-127.

6 M. J. Olszta, D. J. Odom, E. P. Douglas and L. B. Gower, *Connect. Tissue Res*, 2009, 44, 326-334.

7 A.-W. Xu, Y. Ma and H. Cölfen, *J. Mater. Chem*, 2007, 17, 415-449.

8 F. Nudelman, A. J. Lausch, N. A. Sommerdijk and E. D. Sone, *J. Struct. Biol*, 2013, 183, 258-269.

9 D. Wu, J. Yang, J. Li, L. Chen, B. Tang, X. Chen, W. Wu and J. Li, *Biomaterials*, 2013, 34, 5036-5047.

10 J. Sun, C. Chen, H. Pan, Y. Chen, C. Mao, W. Wang, R. Tang and X. Gu, *J. Mater. Chem. B*, 2014, 2, 4544-4553.

11 Y. Z. Zhou, Y. Cao, W. Liu, C. H. Chu and Q. L. Li, *ACS Appl. Mater. Interfaces*, 2012, 4, 6901-6910.

12 D. N. Zeiger, W. C. Miles, N. Eidelman and S. Lin-Gibson, *Langmuir: the ACS journal of surfaces and colloids*, 2011, 27, 8263-8268.

13 W. J. Habraken, J. Tao, L. J. Brylka, H. Friedrich, L. Bertinetti, A. S. Schenk, A. Verch, V. Dmitrovic, P. H. Bomans, P. M. Frederik, J. Laven, P. van der Schoot, B. Aichmayer, G. de With, J. J. DeYoreo and N. A. Sommerdijk, *Nat. Commun*, 2013, 4, 1507.

14 A. George and A. Veis, Chem. Rev, 2008, 108, 4670-4693.

15 M. J. Olszta, X. Cheng, S. S. Jee, R. Kumar, Y.-Y. Kim, M. J. Kaufman, E. P. Douglas and L. B. Gower, *Materials Science and Engineering: R: Reports*, 2007, 58, 77-116.

16 R. P. Sear, *Int. Mater. Rev*, 2013, 57, 328-356.

17 K. Jiao, L.-N. Niu, C.-F. Ma, X.-Q. Huang, D.-D. Pei, T. Luo, Q. Huang, J.-H. Chen and F. R. Tay, *Adv. Funct. Mater*, 2016, 26, 6858-6875.

18 L. N. Niu, W. Zhang, D. H. Pashley, L. Breschi, J. Mao, J. H. Chen and F. R. Tay, *Dent. Mater: official publication of the Academy of Dental Materials*, 2014, 30, 77-96.

19 M. Ekambaram, M. S. Snb and Y. Cky, *Oral Health Prev. Dent*, 2017, 15, 1-6.

20 Y. Cao, M. L. Mei, Q.-L. Li, E. C. M. Lo and C. H. Chu, ACS Appl. Mater. Interfaces, 2013, 6, 410-420.

21 Q. Ruan, Y. Zhang, X. Yang, S. Nutt and J. Moradian-Oldak, *Acta Biomater*, 2013, 9, 7289-7297.

22 M. Oshiro, K. Yamaguchi, T. Takamizawa, H. Inage, T. Watanabe, A. Irokawa, S. Ando and M. Miyazaki, *J. Oral Sci*, 2007, 49, 115-120.

23 M. J. Olszta, E. P. Douglas and L. B. Gower, *Calcif. Tissue Int*, 2003, 72, 583-591.

24 X. Cheng and L. B. Gower, *Biotechnol. Prog*, 2006, 22, 141–149.

25 X. J. Luo, H. Y. Yang, L. N. Niu, J. Mao, C. Huang, D. H. Pashley and F. R. Tay, *Acta Biomater*, 2016, 31, 378-387.

26 L. Zhang, M. D. Weir, L. C. Chow, J. M. Antonucci, J. Chen and H. H. Xu, *Dent. Mater: official publication of the Academy of Dental Materials*, 2016, 32, 285-293.

27 Z. Wu, X. Wang, Z. Wang, C. Shao, X. Jin, L. Zhang, H. Pan, R. Tang and B. Fu, *ACS Appl. Mater. Interfaces*, 2017, 9, 17710-17717.

28 R. A. Giacaman, C. Fernández, C. Muñozsandoval and N. Fuentes, *Oral Health Prev. Dent*, 2017, 1-5.

29 P. A. Keane and S. R. Sadda, *Ophthalmology*, 2014, 121, 2489-2500.

30 M. Koch and V. Ntziachristos, *Annu. Rev. Med*, 2016, 67, 153-164.

31 S. V. Dorozhkin, *Acta Biomater*, 2010, 6, 4457.

Nanoscale Accepted Manuscript

ARTICLE

32   H. Ding, H. Pan, X. Xu and R. Tang, *Cryst. Growth Des*, 2015, 14, 763–769.
33   S. Liu, W. Weng, Z. Li, L. Pan, K. Cheng, C. Song, P. Du, G. Shen and G. Han, *Mater. Sci. Mater. Med*, 2009, 20, 359.
34   F. Nudelman, K. Pieterse, A. George, P. H. Bomans, H. Friedrich, L. J. Brylka, P. A. Hilbers, W. G. De and N. A. Sommerdijk, *Nat. Mater*, 2010, 9, 1004.
35   L. Niu, E. J. Sang, K. Jiao, L. Tonggu, M. Li, L. Wang, Y. Yang, J. Bian, L. Breschi and S. S. Jang, *Nat. Mater*, 2017, 16, 370.
36   D. Rabadjieva, R. Gergulova, R. Titorenkova, S. Tepavitcharova, E. Dyulgerova, C. Balarew and O. Petrov, *Mater. Sci.-Mater. Med*, 2010, 21, 2501-2509.
37   C. Qi, Y. J. Zhu, X. Y. Zhao, B. Q. Lu, Q. L. Tang, J. Zhao and F. Chen, *Chemistry (Weinheim an der Bergstrasse, Germany)*, 2013, 19, 981-987.
38   R. Francis, J. Ariga, M. S. Al, P. Soparkar and A. K. Mascarenhas, *Oral Health Prev. Dent*, 2016, 14.
39   W. Chen, *Acta Phys.-Chim. Sin*, 1986, 2, 400-407.
40   H. Lan, G. Lv, Y. Wen, Y. Mao, C. Huang and T. Yi, *Dyes Pigment*, 2016, 131, 18-23.
41   I. S. Shin, T. Hirsch, B. Ehrl, D. H. Jang, O. S. Wolfbeis and J. I. Hong, *Anal. Chem*, 2012, 84, 9163-9168.
42   L. N. Niu, K. Jiao, H. Ryou, C. K. Yiu, J. H. Chen, L. Breschi, D. D. Arola, D. H. Pashley and F. R. Tay, *Angewandte Chemie*, 2013, 52, 5762-5766.
43   A. L. Rossi, I. C. Barreto, W. Q. Maciel, F. P. Rosa, M. H. Rocha-Leão, J. Werckmann, A. M. Rossi, R. Borojevic and M. Farina, *Bone*, 2012, 50, 301-310.
44   Y. Liu, S. Liu, D. Luo, Z. Xue, X. Yang, L. Gu, Y. Zhou and T. Wang, *Adv. Mater*, 2016, 28, 8740-8748.
45   H. Colfen and S. Mann, *Angewandte Chemie*, 2003, 42, 2350-2365.
46   C. Combes and C. Rey, *Acta Biomater*, 2010, 6, 3362-3378.
47   K. Onuma and M. Iijima, *Sci Rep*, 2017, 7, 2711.
48   S. Jiang, H. Pan, Y. Chen, X. Xu and R. Tang, *Faraday Discuss*, 2015, 179, 451-461.
49   S. Kababya, A. Gal, K. Kahil, S. Weiner, L. Addadi and A. Schmidt, *J. Am. Chem. Soc*, 2015, 137, 990-998.
50   I. Sideridou, V. Tserki and G. Papanastasiou, *Biomaterials*, 2003, 24, 655-665.
51   L. Song, Q. Ye, X. Ge, A. Misra, C. Tamerler and P. Spencer, *Acta Biomater*, 2018, 67, 111-121.
52   J. Fletcher, D. Walsh, C. E. Fowler and S. Mann, *Crystengcomm*, 2011, 13, 3692-3697.
53   A. W. Xu, M. Antonietti, H. Cölfen and Y. P. Fang, Adv. Funct. Mater, 2006, 16, 903-908.
54   A.-W. Xu, M. Antonietti, S.-H. Yu and H. Cölfen, Adv. Mater, 2008, 20, 1333-1338.
55   A.-W. Xu, Y. Ma and H. Cölfen, J. Mater. Chem, 2007, 17, 415-449.
56   C. Y. Wu, D. Young, J. Martel and J. D. Young, Nanomedicine : nanotechnology, biology, and medicine, 2015, 10, 1.
57   P. W. Lucas, S. M. Philip, D. Al-Qeoud, N. Al-Draihim, S. Saji and A. van Casteren, Evol. Dev, 2016, 18, 54-61.
58   L. C. Palmer, C. J. Newcomb, S. R. Kaltz, E. D. Spoerke and S. I. Stupp, Chem. Rev, 2008, 108, 4754-4783.
59   J. Kim, D. D. Arola, L. Gu, Y. K. Kim, S. Mai, Y. Liu, D. H. Pashleyand F. R. Tay, *Acta Biomater*, 2010, 6, 2740-2750.
60   Y. Fan, Z. Sun and J. Moradian-Oldak, Biomaterials, 2009, 30, 478-483.
61   V. Uskokovic, S. Tang and V. M. Wu, ACS Appl. Mater. Interfaces, 2018, 10, 14491-14508.
62   X. Zheng, Y. Wang, Z. Lan, Y. Lyu, G. Feng, Y. Zhang, S. Tagusari, E. Kislauskis, M. P. Robich and S. Mccarthy, J. Biomed. Nanotechnol, 2014, 10, 900-910.
63   D. Gu, G. Feng, G. Kang, X. Zheng, Y. Bi, S. Wang, J. Fan, J. Xia, Z. Wang and Z. Huo, J. Nanomater, 2016, (2016-3-22), 2016, 2016, 1-8.